J. Cent. South Univ. (2019) 26: 984−999
DOI: https://doi.org/10.1007/s11771-019-4065-z

Springer

Strainburst process of marble in tunnel-excavation-induced stress path considering intermediate principal stress

JIANG Bang-you(蒋邦友)[1, 2], GU Shi-tan(顾士坦)[1, 2], WANG Lian-guo(王连国)[3], ZHANG Guang-chao(张广超)[1, 2], LI Wen-shuai(李文帅)[3]

1. State Key Laboratory of Mining Disaster Prevention and Control Co-founded by Shandong Province and the Ministry of Science and Technology, Shandong University of Science and Technology, Qingdao 266590, China;
2. National Demonstration Center for Experimental Mining Engineering Education, Shandong University of Science and Technology, Qingdao 266590, China;
3. State Key Laboratory of Geomechanics and Deep Underground Engineering, China University of Mining and Technology, Xuzhou 221116, China

Abstract: Strainburst is one type of rockburst that generally occurs in deep tunnel. In this study, the strainburst behaviors of marble specimens were investigated under tunnel-excavation-induced stress condition, and two stress paths were designed, a commonly used stress path in true triaxial unloading rockburst tests and a new test path in which the intermediate principal stress was varied. During the tests, a high-speed camera was used to record the strainburst process, and an acoustic emission (AE) monitoring system was used to monitor the AE characteristics of failure. In these two stress paths, all the marble specimens exhibited strainbursts; however, when the intermediate principal stress was varied, the rockburst became more violent. The obtained results indicate that the intermediate principal stress has a significant effect on rockburst behavior of marble. Under a higher intermediate principal stress before the unloading, more elastic strain energy was accumulated in the specimen, and the cumulative AE energy was higher in the rockburst-induced failure, i.e., more elastic strain energy was released during the failure. Therefore, more violent failure was observed: more rock fragments with a higher mass and larger size were ejected outward.

Key words: strainburst; true triaxial test; intermediate principal stress; acoustic emission; marble

Cite this article as: JIANG Bang-you, GU Shi-tan, WANG Lian-guo, ZHANG Guang-chao, LI Wen-shuai. Strainburst process of marble in tunnel-excavation-induced stress path considering intermediate principal stress [J]. Journal of Central South University, 2019, 26(4): 984–999. DOI: https://doi.org/10.1007/s11771-019-4065-z.

1 Introduction

Rockburst is a typical unstable rock failure. Specifically, under high ground-stress conditions, unloading in tunnel excavation would cause stress concentration on hard and brittle rocks around the excavation boundary and trigger a sudden release of elastic stain energy stored in the surrounding rocks, causing failures such as burst, exfoliation, ejection,

Foundation item: Project(2016YFC0801403) supported by the National Key Research and Development Program of China; Project(2017RCJJ012) supported by the Scientific Research Foundation of Shandong University of Science and Technology for Recruited Talents, China; Project(ZR2018MEE009) supported by the Shandong Provincial Natural Science Foundation, China; Project(MDPC2017ZR04) supported by the Open Project Fund for State Key Laboratory of Mining Disaster Prevention and Control Co-founded by Shandong Province and the Ministry of Science and Technology of China
Received date: 2018-05-16; **Accepted date:** 2018-12-06
Corresponding author: GU Shi-tan, PhD, Associate Professor; Tel: +86-532-86058083; E-mail: chinasdgst@163.com; ORCID: 0000-0003-2433-0533

and even high-speed throwing [1–3]. Rockbursts are characterized by locality, abruptness, concealment, hysteresis, no forewarning, high initial velocity, and high-impact kinetic energy and cause heavy causalities and economic loss in underground projects [4–6]. Generally, rockburst can be divided into three types, namely, strainburst, fault-slip rockburst, and coal-pillar rockburst. Strainburst, which is the most prevalent type of rockburst, generally occurs around the tunnel excavation boundary, mainly induced by the local high stress concentration and release of elastic strain energy in excavation [7]. For example, hundreds of strainbursts occurred during the construction of the water diversion tunnel in Jinping II-level hydropower station, which not only caused severe casualties and equipment damage, but also delayed the construction [1, 8, 9].

In recent years, extensive mechanical analysis, laboratory tests, and case statistics have been conducted for strainbursts [10–19]. Mimicking the overall failure process of strainburst in the laboratory has been one of the important ways to elucidate the mechanisms. In order to realistically simulate the stress paths and boundary conditions for rocks during an excavation in which strainburst occurs, HE et al [20] developed a deep-rockburst experimental system using true triaxial testing instruments. During the test, first different stresses in three directions were loaded on the rock specimen, and then a horizontal stress was rapidly loaded while the stresses along the other two directions remained unchanged, or the vertical stress was increased while the horizontal stress remained unchanged, to simulate the stress condition on the rock under excavation disturbance in practical engineering. Using this experimental system, HE et al [10, 21, 22] conducted a series of rockburst tests with different loading/unloading paths and investigated the strainburst behavior of rock under the triaxial unloading condition. ZHAO et al [4] carried out strainburst tests on Beishan granites at four different unloading rates and concluded that, at a higher unloading rate, the rockburst was easily triggered and more violent. Specimen dimension also has an important influence on the bursting behaviour of rock. ZHAO et al [7] conducted triaxial loading/unloading tests on granite specimens with different width-to-height ratios to evaluate their strainburst behavior; the specimen with a smaller width-to-height ratio had a more violent rockburst. Moreover, the cumulative AE energy gradually decreased with the increase in the width-to-height ratio specimen [23]. SU et al [24] also developed a true triaxial stiff testing machine and performed many tests on granite specimens to investigate their strainburst-induced destruction and the effect of tunnel axial stress on rockburst and destruction characteristics. DU et al [25] and HE et al [26] extensively studied strainbursts in different rock specimens under true triaxial unloading and local dynamic disturbance and analyzed the rockburst and AE characteristics under the combined action of triaxial static load and impact dynamic load in depth. AKDAG et al [27] investigate the effects of thermal damage on the strain burst characteristics of brittle rocks under true-triaxial loading-unloading conditions. Based on above researches, a comprehensive database has been created on the true-triaxial unloading tests on strainbursts.

Notably, none of the aforementioned testing methods considered the variation of intermediate principal stress during excavation. However, in a practical tunnel excavation, σ_2 on the rocks around the excavation boundary was not always unchanged.

EBERHARDT [28] conducted 3D numerical simulations on tunnel excavation; when the intermediate principal stress in the initial ground stress field was parallel to the axial direction of tunnel, σ_2 on the surrounding rocks first increased and then decreased as the working face moved forward. As shown in Figure 1, σ_2 reached the maximum when the working face was parallel to the measuring point. According to the field monitoring results of the stress field on the surrounding rocks during the mining of Winston Lake Mine, KAISER et al [29] concluded that σ_2 first increased and then decreased; moreover, after achieving the stability, σ_2 on the surrounding rocks was slightly smaller than the initial ground stress. It is well known that the intermediate principal stress significantly affects the strength and failure characteristics of rocks. And many true triaxial tests show that the effect of intermediate principal stress on rock mechanics is unallowable to be neglected [30]. Therefore, the effect of the variation of intermediate principal stress on the strainburst process and characteristics should be considered.

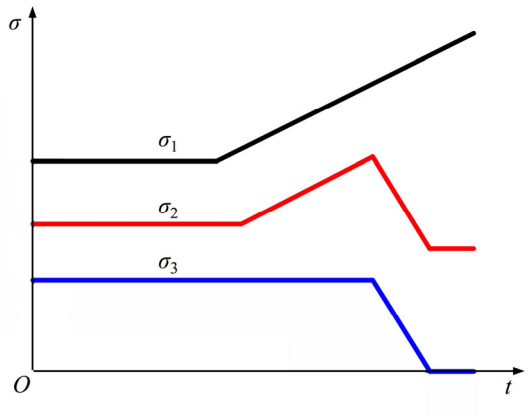

Figure 1 Simplified tunnel-excavation-induced stress path

In this study, true triaxial tests were conducted to investigate the strainburst of marble specimens in tunnel-excavation-induced stress path. Compared to previous studies, this study considered the effect of the variation of intermediate principal stress on the surrounding rocks on strainburst during the tunnel excavation. During the tests, the marble specimens were first subjected to the initial 3D stress state and then σ_3 remained unchanged while σ_1 and σ_2 were increased to the preset values. Next, σ_1 was further increased, but σ_3 was gradually decreased to 0 and σ_2 was gradually increased to the preset value. σ_1, σ_2, and σ_3 were changed as described above for simulating the stress paths on the tunnel surrounding rocks during the excavation. A high-speed camera was used to record the strainburst, and an AE monitoring system was used to detect the AE signals in strainburst in real time. In the rest of this paper, first the basic parameters of the marble specimen, true triaxial testing system used in this study, and specific test process were first introduced, and then the strainburst process and characteristics of specimen under tunnel excavation stress path were analyzed in detail. Furthermore, the effect of intermediate principal stress on strainburst behavior was analyzed.

2 Test method

2.1 Specimen preparation

Cyan marble specimens were used in this study; they were compact and uniform at a microlevel with a high crystallinity and hardness. Table 1 shows the basic physicomechanical parameters of the marble.

Table 1 Mechanical properties of marble material used in this study

Property	Value
Density, ρ/(kg·m^{-3})	27.1
Elastic modulus, E/GPa	25.3
Poisson ratio, υ	0.20
Uniaxial compressive strength, σ_c/MPa	89.6
Internal cohesion, c/MPa	21.4
Internal frictional angle, φ/(°)	38.1

Rectangular prism specimens with a size of 50 mm×50 mm×100 mm were cut from a large marble stone. To reduce the end-surface effects, the end surfaces of each specimen were polished so that the flatness of each end surface was 0.1 mm, and the adjacent surfaces were as perpendicular as possible. To reduce the effects of nonuniformity and initial damage on the test results, the prepared specimens were further screened using a digital intelligent acoustic detector. 15 marble specimens were selected; they were divided into five groups for tests. Table 2 shows the grouping of the specimens and basic physical parameters. The average P-wave velocity of all the rock specimens was 4803 m/s.

2.2 True triaxial rockburst testing system

The used true triaxial rockburst testing system was designed and developed by State Key Laboratory of Geomechanics and Deep Underground Engineering, China University of Mining and Technology, as shown in Figure 2. The stiffness along the X, Y and Z directions exceeded 5 mN/mm. The maximum pressures along the X, Y and Z directions were 300, 500 and 2000 kN, respectively. And the testing system was equipped with an advanced high-speed camera and AE monitoring system to monitor the entire rockburst process and AE signal characteristics. The high-speed camera has a maximum shoot speed of 2000 frames per second; the AE sensor has a cross-section diameter of 8 mm and a frequency range of 100–900 kHz. During the tests, the AE signals were amplified using a preamplifier with a gain of 40 dB. In the AE monitoring system, the sampling frequency was set as 3 M per second; the lockout time of AE events and threshold value were set as 100 μs and 30 mV, respectively.

In the true triaxial tests on rocks, HE et al

Table 2 Basic physical parameters of marble specimens

Group	Specimen number	Specimen size/(mm×mm×mm)	Mass, M_s/g	Density/(g·cm^{-3})	P-wave speed/(m·s^{-1})
G1	G1-1	50.83×49.96×101.28	701.14	2.73	4762
	G1-2	50.76×50.03×101.53	696.14	2.70	4795
	G1-3	50.67×49.86×101.26	695.86	2.72	4722
G2	G2-1	49.99×50.51×101.71	696.97	2.71	4843
	G2-2	49.52×50.41×101.37	690.67	2.73	4827
	G2-3	50.40×49.62×101.61	682.94	2.69	4839
G3	G3-1	50.17×49.72×100.47	684.11	2.73	4764
	G3-2	49.92×49.90×101.42	685.71	2.71	4830
	G3-3	49.73×49.95×101.50	686.71	2.72	4833
G4	G4-1	50.43×49.97×101.38	702.25	2.75	4828
	G4-2	50.65×49.46×101.16	694.53	2.74	4817
	G4-3	50.71×49.56×101.36	694.70	2.73	4821
G5	G5-1	49.68×49.79×101.49	681.36	2.71	4768
	G5-2	49.83×50.05×101.32	696.15	2.72	4795
	G5-3	49.89×49.99×101.24	688.87	2.71	4820

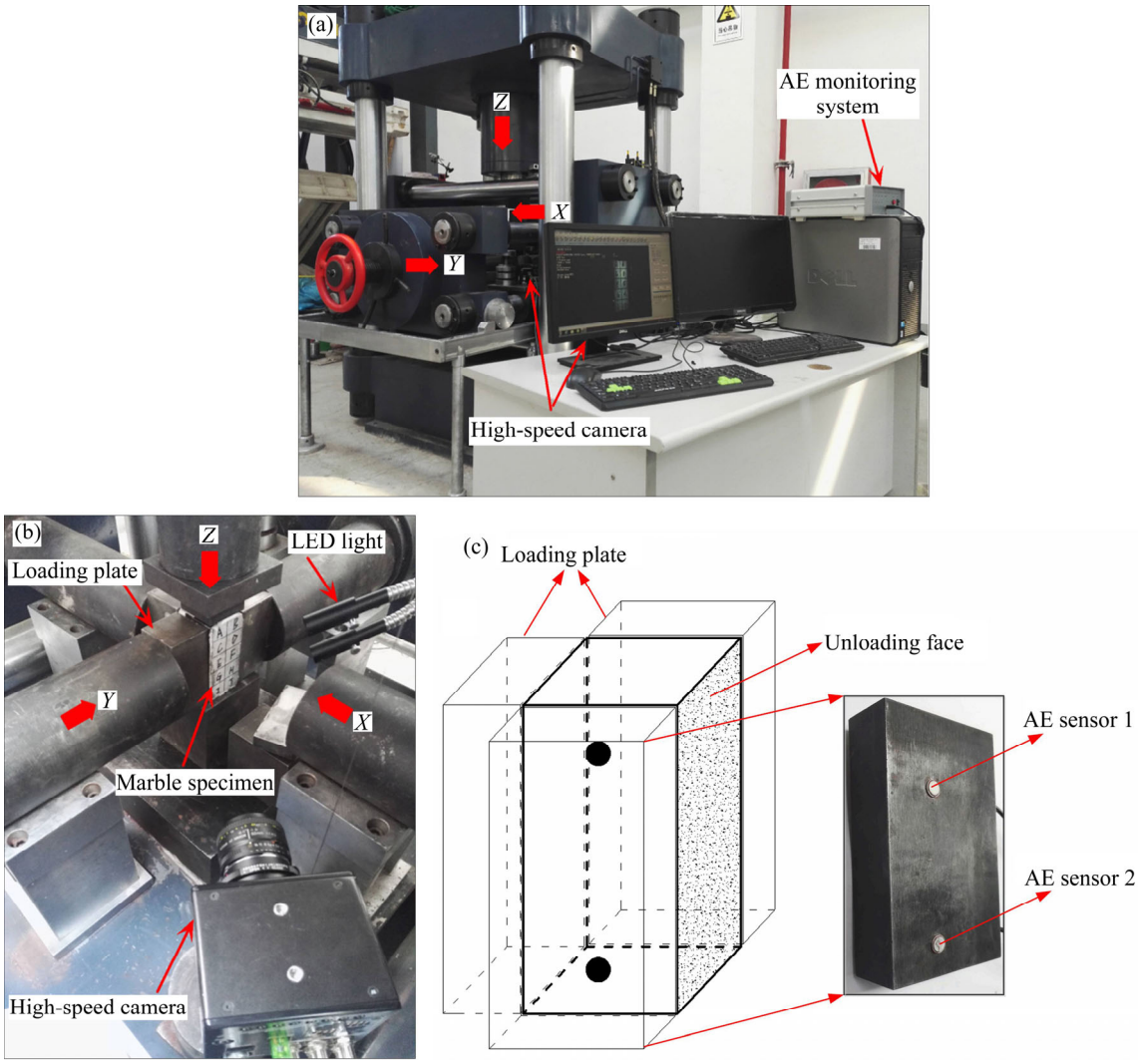

Figure 2 Ture-triaxial rockburst testing system: (a) Composition of testing system; (b) Internal structure and loading mode; (c) Positions of AE sensors

[10, 21] arranged the AE sensor on the plate in contact with the specimen. Therefore, before reaching the sensor, the AE signals generated during the failure in the rocks passed through several media made of different materials, thus significantly affecting the monitoring precision. To enhance the AE monitoring precision, a loading plate mounted with an AE sensor was specially designed in this study. As shown in Figure 2(c), a small spring was placed on the back of the AE sensor. Therefore, not only the tight contact between the probe and specimen can be guaranteed, but also the damage to the sensor caused by large forces can be avoided.

Besides, the noises generated due to the friction between the specimen and loading plate as well as that between the pressuring plate and head also significantly hindered the analysis and receiving of AE signal induced by the failure in the rock [31]. A mixture of vaseline and stearic acid with a mass ratio of 1:1 was used in this study to reduce the friction effects [32, 33]. On one hand, the abovementioned frictions as well as the friction effects among various end surfaces were eliminated, but also the friction-induced noise was minimized. The mixture was prepared by heating vaseline and stearic acid on a water bath.

2.3 Testing process

2.3.1 Design of stress paths for strainburst test

As shown in Figure 1, EBERHARDT [28] and KAISER et al [29] found that σ_2 on excavation boundary rocks was not fixed, but first increased and then decreased with the advance of working face in tunnel excavation. Currently, in most rockburst tests, the effects of the loading rates of σ_1 and σ_3, rock stratification direction, and specimen size on rockburst process and AE characteristics were investigated. The value of σ_2 was unchanged, and its effect on the rockburst test results under practical excavation stress paths was not considered.

Therefore, two different stress paths were designed for this laboratory strainburst test, as shown in Figure 3. Stress path A was designed based on the excavation stress path shown in Figure 1, in which the variation of σ_2 in tunnel excavation was considered. In contrast, stress path B was commonly used in the current rockburst tests, in which σ_2 remained unchanged during the unloading. This was the only difference between these two paths. In Figure 3, σ_{1o}, σ_{2o}, and σ_{3o} are the three principal stresses corresponding to the initial ground stress; σ_{1a} and σ_{2a} are the concentrated stresses of the maximum stress and intermediate stress before the excavation. They were related to the concentration degree of stress on the surrounding rocks before the excavation. v_{l1} and v_{l2} are the loading rates of σ_1 and σ_2, respectively. v_{u2} and v_{u3} are the unloading rates of σ_2 and σ_3, respectively, heavily dependent on the excavation mode and rate. t_1–t_3 are the stress concentration phases induced by tunnel excavation; finally, the tunnel-excavation-induced stress was unloaded.

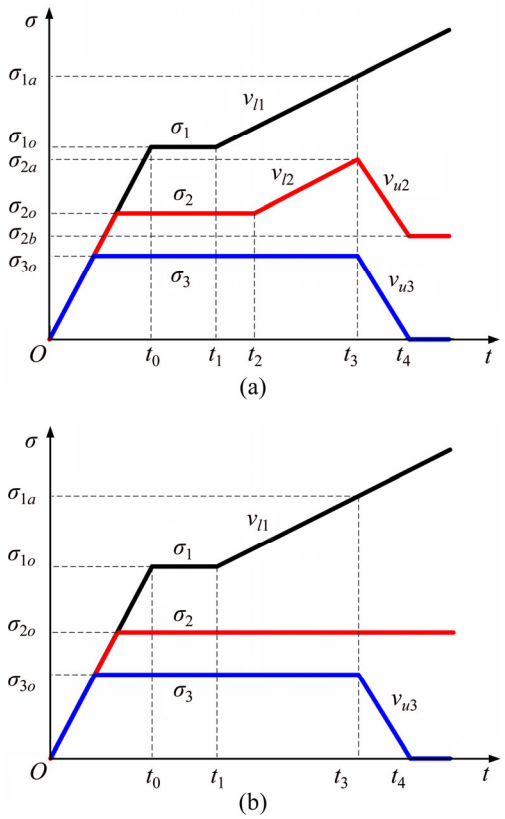

Figure 3 Stress plan in strainburst test: (a) Test plan A; (b) Test plan B

2.3.2 Initial ground stress condition

Before the strainburst tests, the ground stress condition triggering the rockburst should be determined. This study focused on the strainbursts during the construction of water diversion tunnels in Jinping II-level hydropower station. For the four water diversion tunnels, the average burial depth was 1900 m. According to the statistics of rockbursts on the construction site, flakiness and continuous rockbursts occurred most frequently in

the marbles of Baishan formation. The marbles of Baishan formation are characterized by a high structural integrity and compaction, with a natural uniaxial compressive strength of 55–114 MPa and an elastic modulus of 25–40 GPa. They are similar to marble specimens used in this study in terms of mechanical properties. The field ground stress test and inversion results show that the maximum, intermediate, and minimum principal stresses at an elevation of 1900 m were 56.96, 49.64 and 43.36 MPa, respectively [9]. To achieve the loading and unloading in the tests, the values of σ_{1o}, σ_{2o}, and σ_{3o} under the initial ground stress condition in stress paths A and B were set as 57, 50 and 43 MPa, respectively.

2.3.3 Detailed test processes

To investigate the strainburst and AE characteristics under tunnel excavation paths in depth, a detailed test procedure was designed, in which the directions of σ_1, σ_2, and σ_3 corresponded to the Z, Y and X directions of the true triaxial testing instrument. The specific testing procedures are described below:

1) Setting of initial ground stress condition. The specimen was loaded along the directions of three ground stresses at a loading rate of 0.5 MPa/s until the loads in the three principal stress directions reached the initial ground stress condition (i.e., the stress condition at t_0 shown in Figure 3). Next, the principle stresses along the three directions remained unchanged and lasted for a certain time.

2) Tunnel-excavation-induced strainburst tests. As described above, two stress paths were designed in this study to trigger rockbursts. As shown in Figure 3(a), for stress path A, the loads in the directions of σ_1 and σ_2 first increased to σ_{1a} and σ_{2a} at rates of v_{l1} and v_{l2}, respectively, while the load in the direction of σ_3 remained unchanged. Then, the loads in the directions of σ_2 and σ_3 were decreased to σ_{2b} and 0 at rates of v_{u2} and v_{u3}, respectively, and then remained unchanged. Finally, the stresses in the directions of σ_2 and σ_3 were unloaded, while the load in the direction of σ_1 was further increased until the rockburst occurred. For stress path B, the loading/unloading process was basically similar to that under stress path A; the only difference was that σ_2 remained unchanged during the entire process, as shown in Figure 3(b).

LIU [34] conducted numerical simulations for the stress on the tunnel wall surrounding rocks in Jinping II-level hydropower station and determined the stress distribution rules with the advance of working face. They found that when the working face was parallel to the measuring point, the stress concentration factors of σ_1 and σ_2 of the surrounding rocks at the measuring point were 1.52–1.57. Therefore, in these tests, σ_{1a} and σ_{2a} were set as 90 MPa and 75 MPa, respectively. To further evaluate the effect of intermediate principal stress σ_{2a} on the rockburst process and characteristics, three sets of tests were conducted, where σ_{2a} was set to different values (70, 65 and 60 MPa, respectively) and the other parameters were fixed. Four sets of tests were performed using stress path A, and each test was repeated three times. For comparison, only one set of test was performed using stress path B. Table 3 shows the specific test grouping results. In this study, the effects of loading and unloading rates on the rockburst process and characteristics were not considered. Therefore, v_{l1} and v_{l2} were set as 0.5 MPa/s, and v_{u2} and v_{u3} were set as –0.5 MPa/s.

Table 3 Testing plan of marble specimens

Group	Test plan	σ_{1a}/ MPa	σ_{2a}/ MPa	σ_{2b}/ MPa	v_{l1}, v_{l2}/ (MPa·s^{-1})	v_{u2}, v_{u3}/ (MPa·s^{-1})
G1	Test plan A	90	75	30	0.5, 0.5	–0.5, –0.5
G2		90	70	30	0.5, 0.5	–0.5, –0.5
G3		90	65	30	0.5, 0.5	–0.5, –0.5
G4		90	60	30	0.5, 0.5	–0.5, –0.5
G5	Test plan B	90	50	50	0.5, —	—, –0.5

3 Test result and discussion

In this section, the rockburst test results of five sets of 15 specimens are presented and analyzed. Because of the limitation of paper length, one typical specimen was selected from each set of test, and five typical specimens in total were selected from five sets of tests. Figure 4 shows the actual stress paths, AE counts, and cumulative AE energy values of these five typical specimens in the tests; the relationship between cumulative AE energy and time was plotted in the natural logarithm-linear (ln-linear) form. The actual stress paths in the tests fit well with the designed paths as shown in Figure 3. And the test results of 15 specimens under the designed paths are listed in Table 4. To investigate the strainburst process and

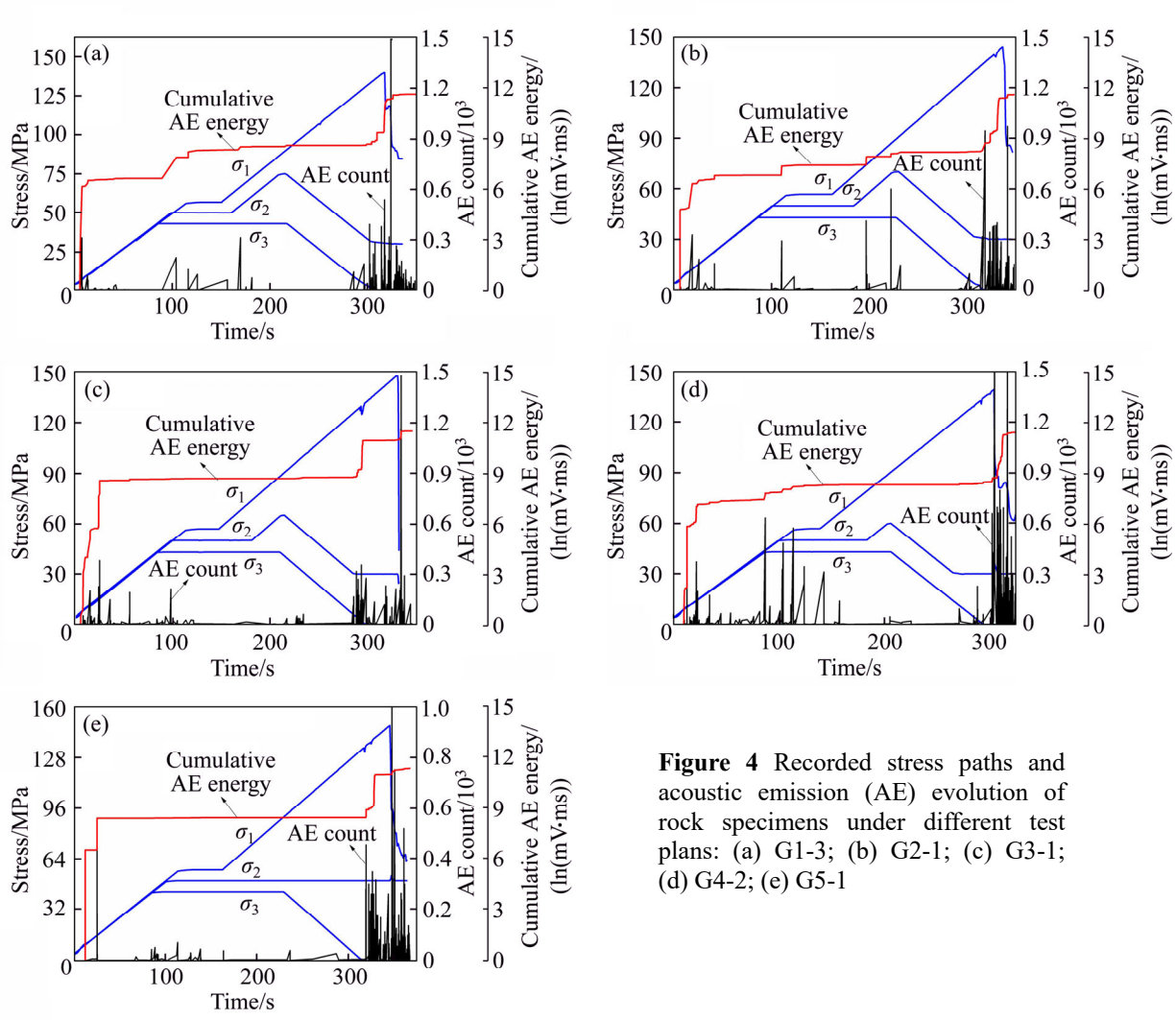

Figure 4 Recorded stress paths and acoustic emission (AE) evolution of rock specimens under different test plans: (a) G1-3; (b) G2-1; (c) G3-1; (d) G4-2; (e) G5-1

Table 4 Test results of marble specimens

Group	Specimen number	σ_2/MPa	σ_3/MPa	σ_1 at failure/MPa	Duration time of strainburst process/s
G1	G1-1	50↗75↘30	43→0	136	7.3
	G1-2	50↗75↘30	43→0	155	3.8
	G1-3	50↗75↘30	43→0	140	2.0
G2	G2-1	50↗70↘30	43→0	144	4.8
	G2-2	50↗70↘30	43→0	160	4.4
	G2-3	50↗70↘30	43→0	132	8.9
G3	G3-1	50↗65↘30	43→0	148	8.1
	G3-2	50↗65↘30	43→0	137	17.8
	G3-3	50↗65↘30	43→0	141	3.5
G4	G4-1	50↗60↘30	43→0	159	9.0
	G4-2	50↗60↘30	43→0	139	5.8
	G4-3	50↗60↘30	43→0	128	1.2
G5	G5-1	50	43→0	148	—
	G5-2	50	43→0	166	—
	G5-3	50	43→0	154	—

characteristics of marble under tunnel excavation stress paths, the test results were analyzed in depth from the following three aspects: rockburst destruction process, ejection of rock fragments, and AE characteristics.

3.1 Failure process of strainburst

A high-speed camera was used in the tests to record the destruction processes of all the marble specimens. To observe the overall destruction characteristics of the specimens more clearly, first the high-speed photographs of each specimen taken in typical destruction stages should be screened. Figure 5 shows the high-speed records of the destruction processes of five typical specimens. Apparently, strainbursts to different degrees were observed in all the specimens. To be specific, fine particles were first ejected from the specimen's unloading free surface. Then, splitting failure occurred on the free surface along the direction parallel to σ_1–σ_2; the rock plates were formed and underwent shearing fracture to form a large number of rock blocks. Finally, the rock blocks were thrown or even ejected outward. Figure 5 also shows that the strainburst process can be divided into four stages: (i) ejection of fine grains, (ii) splitting of rock into plates, (iii) shearing of rock plate into blocks, and (iv) ejection of rock blocks. The total duration time of four stages of strainburst process was different, and exhibited no obvious regularity, as shown in Figure 6. When the rock plates were sheared into blocks, the ejection should be completed very fast within dozens of milliseconds. This shows that the elastic strain energy is accumulated over a long time, but released in an instant; moreover, the higher the release rate of elastic strain energy, the higher the risk of rockburst.

The specimens also showed different rockburst destruction behaviors under two different stress paths. As shown in Figure 5(a), under stress path A, the destructions of specimen G1-3 was very violent, and the entire destruction process was thunderous. A large number of rock blocks were ejected outward from the unloading free surface at a high initial velocity, and some rockburst notches were formed below the free surface. In contrast, as shown in Figure 5(e), under stress path B, specimen G5-1 underwent more gentle destruction, and no obvious ejection of rock blocks was observed. In addition, for the four sets of specimens under stress path A (G1, G2, G3 and G4), σ_2 before the unloading was set as different values (i.e., σ_{2a} was set as different values). Therefore, their rockburst destruction behaviors also showed significant differences. When σ_{2a}=75 MPa, the specimen underwent intensive destruction, and the generated rock blocks were instantaneously ejected from the unloading free surface at a high velocity (Figure 5(a)). When σ_{2a}=70 MPa, an obvious strainburst was observed. The rock blocks formed in the shearing destruction at the top of unloading free surface were ejected outward at a high velocity, and a large amount of elastic strain energy was released (Figure 5(b)). When σ_{2a}=65 MPa, the specimen also ejected small rock grains, rocks splitted into plates, plates sheared into blocks, and blocks were ejected, but the destruction intensity and ejection velocity of rock blocks were significantly smaller than those of specimens G1 and G2 (Figure 5(c)). When σ_{2a}=60 MPa, the specimen experienced peeling destruction rather than intensive strainburst, i.e., the rock plates formed in splitting failure were peeled off and dropped from the unloading free surface of the specimen more gently and only some small rock plates were slightly ejected (Figure 5(d)). This indicates that the larger the σ_{2a}, the faster the ejection velocity of rock blocks when strainburst occurs. Based on the abovementioned observations, the intermediate principal stress significantly affected the strainburst of marble. Under the tunnel-excavation-induced stress path considering the variation of intermediate principal stress, the specimen exhibited more intensive strainburst process; moreover, with the increase in σ_{2a} the destruction on the unloading free surface of specimen gradually changed from slight ejection and mild exfoliation to violent ejection. This can also be explained from the energy perspective. XIE et al [35] investigated the energy release trend in the destruction process under loading; under triaxial compressive stresses, the elastic strain energy stored in the rock was first released along the direction of σ_3, thus triggering the destruction on the entire rock. The surface energy for the overall destruction of rock, denoted as U_f, can be expressed as follows:

Figure 5 Strainburst process of rock specimens under different test plans: (a) G1-3; (b) G2-1; (c) G3-1; (d) G4-2; (e) G5-1

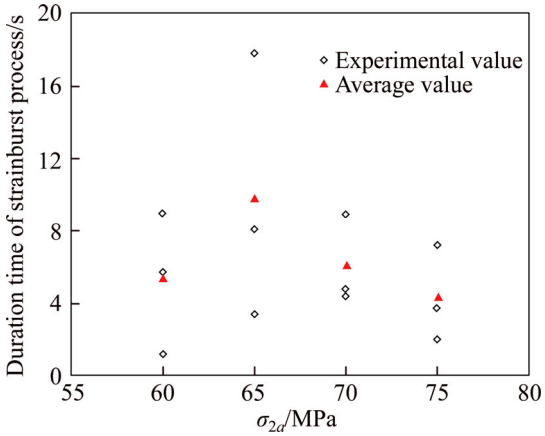

Figure 6 Total duration time of four stages of strainburst process with different σ_{2a}

$$U_f = \frac{\sigma_c^3}{2E(\sigma_1 - \sigma_3)} \quad (1)$$

where σ_c is the uniaxial compressive strength of rock; E is the elasticity modulus of rock; σ_1 and σ_3 are the maximum and minimum principal stresses of rock at failure, respectively. The σ_c and E is constant for the same rock material. And Table 4 shows that the σ_3 at failure of all the 15 marble specimens of Group G1-G5 is the same. According to Eq. (1), without considering the discreteness of specimens, theoretically the surface energies for the overall destruction of all the 15 marble specimens are approximate identical.

Based on the elastic mechanics theory, the elastic strain energy density of rock U_e under triaxial stresses can be expressed as follows:

$$U_e = \frac{\sigma_1^2 + \sigma_2^2 + \sigma_3^2 - 2\nu(\sigma_1\sigma_2 + \sigma_1\sigma_3 + \sigma_2\sigma_3)}{2E} \quad (2)$$

where ν is the Poisson ratio of rock and σ_2 is the intermediate principal stress.

According to the principle of energy conservation, the elastic strain energy released from the destruction of rocks, denoted as U_o, can be expressed as follows:

$$U_o = U_e - U_f - U_c \quad (3)$$

where U_c is the energy dissipation generated in the destruction process of rock such as electromagnetic radiation. U_c is relatively small compared with U_e and U_f, and thus can be neglected.

According to Eq. (2), the elastic strain energy density of rock under triaxial stress condition is related to the intermediate principal stress. Figure 7 shows the variation in the cumulative elastic strain energy density with the intermediate principal stress based on Eq. (2). As can be seen from Figure 7, when σ_1 and σ_3 are fixed, the elastic strain energy density increases with the increase in intermediate principal stress.

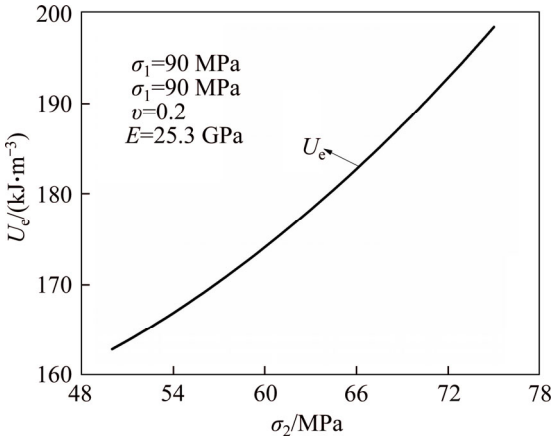

Figure 7 Deformation curve of elastic strain energy density with intermediate principal stress increasing

In conclusion, when energy dissipation such as radiation energy in the destruction process of rock is neglected, more elastic strain energy accumulates in the marble specimen under a higher value of σ_{2a} before the unloading, and more releasable elastic strain energy is stored in the specimen. And then the destruction process will become more violent, which is consistent with the real test phenomena observed by the high-speed camera.

3.2 Ejection of rock fragments in strainburst

The ejection characteristics of rock fragments reflect the failure mechanism in a rockburst to a certain degree. Extensive studies have been conducted on rockburst mechanism in many aspects including the shape of rock fragments, ejection velocity, scale distribution, and microscopic structure. In this study, the ejected rock fragments of each specimen in rockburst processes were collected; they were divided into four groups according to the particle size, namely, microfragments (d<0.075 mm), fine fragments (0.075 mm<d<5 mm), medium fragments (5 mm<d<30 mm), and coarse fragments (d>30 mm). Figure 8 shows the specific grouping results. These fragments show three different shapes. Most of them were flaky fragments, and a small part was irregular lenticel or blocky fragments. To quantitatively analyze the size distribution

Figure 8 Fragments of marble specimens after strainburst: (a) d<0.075 mm; (b) 0.075 mm<d<5 mm; (c) 5 mm<d< 30 mm; (d) 30 mm<d

characteristics of rock fragments produced in rockbursts under tunnel-excavation-induced stress paths, the mass ratios of the fragments with different sizes from each specimen were analyzed. The results are shown in Table 5. Under stress path B, the average total mass of fragments was 41.64 g. Under stress path A, the averages total mass of fragments for group G1–G4 were 47.44, 49.25, 58.51 and 74.46 g, respectively. Under stress path B, the total mass of fragments was obviously smaller than that under stress path A.

Figure 9 shows the variations in distribution of fragments with different σ_{2a}. Under stress path A, when σ_{2a}=60 MPa (group G4), the average mass ratios of entire fragments to specimen was 6.80%, and the average mass ratio of microfragments and fine fragments to entire fragments was 7.17%. When σ_{2a}=75 MPa (group G1), the average mass ratios of entire fragments to specimen increased to 10.67%, but the average mass ratios of microfragments and fine fragments to entire fragments decreased to 4.14 %. As σ_{2a} increased, the ejected rock fragments occupied a higher mass ratio to the total specimen during the rockburst failure. Meanwhile, the microfragments and fine fragments occupied decreasingly smaller mass ratios in the entire fragments, but the mass ratios of medium and coarse fragments gradually increased. When σ_{2a} increased from 60 MPa to 75 MPa, the average mass ratios of microfragments and fine fragments to entire fragments decreased by about 3.87%, but correspondingly the mass ratios of medium and coarse fragments increased by about 3.03%. The rockburst failure characteristics of different

Table 5 Mass ratios of fragments with different sizes of marble specimens during strainburst

Group	Specimen number	Total mass of fragments, M_f/g	Total mass ratio/%	Mass ratio of microfragments/%	Mass ratio of fine fragments/%	Mass ratio of medium fragments/%	Mass ratio of coarse fragments/%
G1	G1-1	66.551	9.492	0.113	5.892	11.798	82.197
	G1-2	69.143	9.932	0.146	3.558	6.656	89.640
	G1-3	87.680	12.600	0.102	2.608	5.845	91.445
G2	G2-1	58.960	8.459	0.120	4.693	15.158	81.029
	G2-2	64.442	9.330	0.143	4.027	7.833	87.997
	G2-3	52.137	7.634	0.109	2.900	12.133	84.857
G3	G3-1	43.498	6.358	0.166	3.961	14.695	81.178
	G3-2	55.268	8.060	0.157	4.979	9.454	85.409
	G3-3	48.993	7.134	0.208	4.825	16.374	78.593
G4	G4-1	50.822	7.237	0.279	5.798	21.624	72.297
	G4-2	43.496	6.263	0.508	8.649	18.038	72.804
	G4-3	47.988	6.908	0.333	5.931	19.096	74.639
G5	G5-1	43.876	6.439	0.444	6.892	21.919	70.745
	G5-2	44.239	6.355	0.298	5.658	14.200	79.844
	G5-3	36.792	5.341	0.465	8.040	27.577	63.919

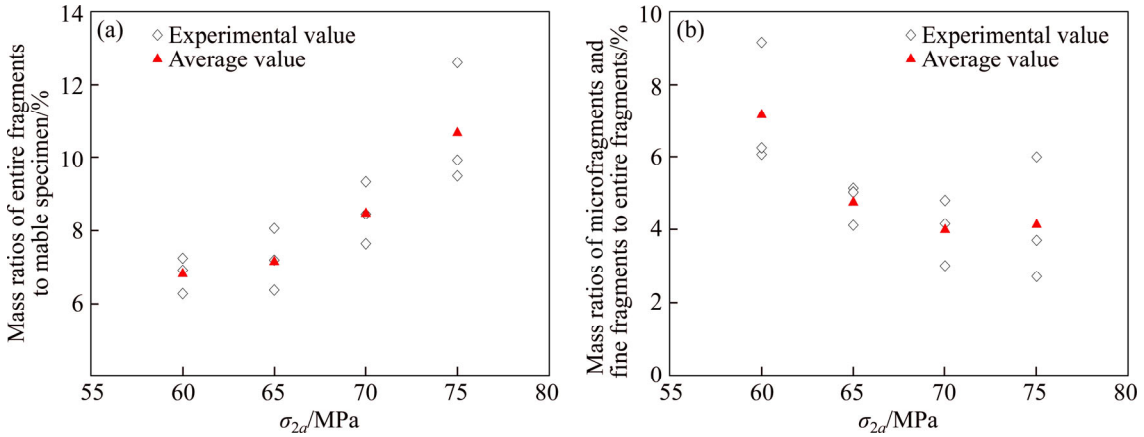

Figure 9 Variations in distribution of fragments with different σ_{2a}: (a) Mass ratios of entire fragments to specimen; (b) Mass ratios of microfragments and fine fragments to entire fragments

specimens were compared. At a higher value of σ_{2a} before unloading, the rockburst failure was more intense, and more fragments with higher masses and larger sizes were ejected.

3.3 AE characteristics in strainbursts

Different stages in the deformation-induced failure of rock showed different AE characteristics [36–38]. As previously reported, the AE count can well characterize the fracture degree in the rock, and cumulative AE energy can accurately reflect the energy release trends in the deformation-induced failure of rock [7, 39, 40]. Therefore, using AE, the strainburst process, AE count, and cumulative AE energy of each marble specimen were measured in real time to gain an in-depth understanding of the failure characteristics and energy release trends of specimen under tunnel excavation stress paths.

As shown in Figures 6(a)–(d), under stress path A, the marble specimens (denoted as G1–G4) show similar variation trends of AE count and cumulative AE energy. According to the relationships of AE count and cumulative AE with time, the AE behaviors of the marble specimens during the strainburst processes can be divided into three typical stages: the initial growth stage, silence stage, and outburst stage. At the initial growth stage, the AE signals were mainly generated in the compaction and closing of the pre-existing fractures as well as in the contact and occlusion between the

fracture surfaces, and no new fractures were produced. The initial growth stage was followed by the silence stage, which corresponded to the elastic energy storage stage of the marble specimen. The specimen underwent elastic deformation, the AE events were relatively silent, and the cumulative AE energy slightly increased. At the outburst stage, a large number of AE events with high counts occurred, and the cumulative AE energy rapidly increased, thus triggering the strainburst. When the strainburst occurred, both the count of AE events and cumulative AE energy reached the maxima. Before the occurrence of strainburst failure, the AE events rapidly increased; this can be regarded as the early warning sign of the occurrence of strainburst.

Figure 4(e) shows that under stress path B, the trends of AE count and cumulative AE energy of the marble specimen (G5) were similar to those under stress path A. Thus, it can be concluded that the variation in intermediate principal stress slightly affected the overall trend of AE events in the strainburst process. However, as shown in Figure 4, the variation in the intermediate principal stress imposed certain effect on the amplitude of cumulative AE energy; the cumulative AE energy varied with the variation in σ_{2a} before the unloading. The cumulative AE energy recorded at the initial growth and silent stages of AE should be deducted from the total cumulative AE energy when analyzing the effects of the variation of intermediate principal stress on cumulative AE energy. This is because the AE events were induced by the compaction and closing of the original fractures, and no new fractures were produced and developed. Therefore, the cumulative AE energy of the marble specimen in rockburst failure was obtained. Under stress path B, the average cumulative AE energy in the failure process of specimen was 85391 mV·ms. Under stress path A, the averages cumulative AE energy for group G1–G4 were 87492, 89703, 103416 and 111404 mV·ms, respectively. Under stress path B, the cumulative AE energy in the failure process of specimen was obviously smaller than that under stress path A. Figure 10 shows the trends of cumulative AE energy in the failure process of specimen with the increase in σ_{2a} before the unloading. This indicates that the cumulative AE energy was higher at a higher σ_{2a} before the unloading. When σ_{2a} increased from 60 MPa to 75 MPa, the cumulative AE energy increased about by 15.9 %. In other words, with the increase in σ_{2a}, the cumulative AE energy of specimen in the failure process increased. More elastic strain energy was released from the specimen, and the corresponding failure process was more violent. This is consistent with the analysis results of rockburst characteristics.

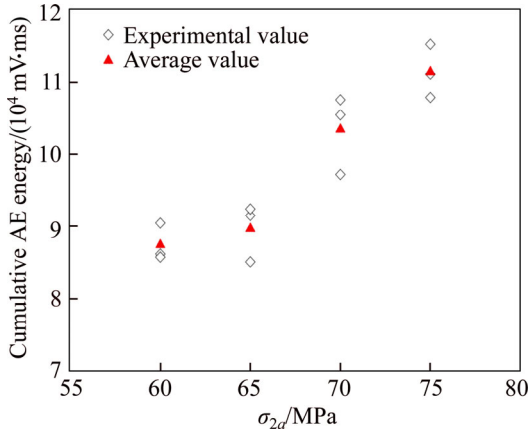

Figure 10 Cumulative AE energy during rock specimens failure process under different σ_{2a}

4 Conclusions

Strainburst is a common dynamic disaster during the excavation of deep and hard tunnels. It is very important to gain the in-depth knowledge of strainburst process and the corresponding behavior characteristics in tunneling excavation. In this study, true triaxial tests were performed on marbles under tunnel-excavation-induced stress paths to investigate the strainburst process. In addition, the tests were also conducted under a common-used stress path in current true triaxial rockburst tests for comparison. During the tests, the self-developed true triaxial testing instrument was used, and high-speed camera and AE monitoring system were also used to record and monitor the rockburst process and generated AE signals. The main conclusions are as follows:

1) All the 15 marble specimens under two different stress paths showed strainbursts to different degrees. The specific process can be divided into four stages: (i) ejection of fine grains, (ii) splitting of rock into plates, (iii) shearing of rock plate into blocks, and (iv) ejection of rock blocks.

2) The intermediate principal stress has a significant effect on the strainburst behavior of marble specimen. After the variation in the

intermediate principal stress was considered, the specimen showed more intense rockburst under tunnel-excavation-induced stress paths. With the increase in the peak of the intermediate principal stress before the unloading (σ_{2a}), the failure on the unloading surface of specimen gradually changed from slightly ejected and mild exfoliation failure to violent ejection failure. This study also elucidated the mechanism from the perspective of energy. When a higher intermediate principal stress was applied on the specimen, more releasable elastic strain energy was accumulated in the specimen, thus showing more violent failure.

3) According to the ejection characteristics of the produced rock fragments, the higher the σ_{2a} was, the more the fragments masses and the larger sizes were ejected. And the similar impacts were obtained in the acoustic emission monitoring of stainburst. The cumulative AE energy gradually increases with the increase of the σ_{2a}. When σ_{2a} increased from 60 MPa to 75 MPa, the average mass ratios of entire fragments to specimen increased about by 3.87%, the average mass ratios of microfragments and fine fragments decreased about by 3.03%, and the cumulative AE energy increased about by 15.9 %.

References

[1] COOK N G W. A note on rockburst considered as a problem of stability [J]. Journal of the South African Institute of Mining and Metallurgy, 1965, 65: 437–446.

[2] GU Shi-tan, JIANG Bang-you, PAN Yue, LIU Zheng. Bending moment characteristics of hard roof before first breaking of roof beam considering coal seam hardening [J]. Shock and Vibration, 2018: Article ID 7082951. DOI: https://doi.org/10.1155/2018/7082951.

[3] ZHAO Tong-bin, GUO Wei-yao, TAN Yun-liang, LU Cai-ping, WANG Cheng-wu. Case histories of rock bursts under complicated geological conditions [J]. Bulletin of Engineering Geology and the Environment, 2017, 77(4): 1529–1545. DOI: https://doi.org/10.1007/s10064-017-1014-7.

[4] ZHAO X G, WANG J, CAI M, CHENG C, MA L K, SU R, ZHAO F, LI D J. Influence of unloading rate on the strainburst characteristics of Beishan granite under true-triaxial unloading conditions [J]. Rock Mechanics and Rock Engineering, 2014, 47: 467–483. DOI: https://doi.org/10.1007/ s00603-013-0443-2.

[5] LEE S M, PARKB B S, LEE S W. Analysis of rockbursts that have occurred in a waterway tunnel in Korea [J]. International Journal of Rock Mechanics and Mining Sciences, 2004, 41(3): 911–916. DOI: https://doi.org/10.1016/j.ijrmms.2003.12.135.

[6] NING Jian-guo, WANG Jun, JIANG Jin-quan, HU Shan-chao, JIANG Li-shuai, LIU Xue-sheng. Estimation of crack initiation and propagation thresholds of confined brittle coal specimens based on energy dissipation theory [J]. Rock Mechanics and Rock Engineering, 2018, 51: 119–134. DOI: https://doi.org/10.1007/s00603-017-1317-9.

[7] ZHAO X G, CAI M. Influence of specimen height-to-width ratio on the strainburst characteristics of Tianhu granite under true-triaxial unloading conditions [J]. Canadian Geotechnical Journal, 2015, 52: 890–902. DOI: 10.1139/cgj-2014-0355.

[8] SHAN Z G, YAN P. Management of rock bursts during excavation of the deep tunnels in Jinping II Hydropower Station [J]. Bulletin of Engineering Geology and the Environment, 2010, 69(3): 353–363. DOI: https://doi.org/10.1007/s10064-010-0266-2.

[9] ZHANG Chuan-qing, FENG Xia-ting, ZHOU Hui, QIU Shi-li, WU Wen-pin. A top pilot tunnel preconditioning method for the prevention of extremely intense rockbursts in deep tunnels excavated by TBMs [J]. Rock Mechanics and Rock Engineering, 2012, 45(3): 289–309. DOI: https://doi.org/10.1007/ s00603-011-0199-5.

[10] HE M C, MIAO J L, FENG J L. Rock burst process of limestone and its acoustic emission characteristics under true-triaxial unloading conditions [J]. International Journal of Rock Mechanics and Mining Sciences, 2010, 47(2): 286–298. DOI: https://doi.org/10.1016/j.ijrmms.2009.09.003.

[11] TAN Y L, YU F H, NING J G, ZHAO T B. Design and construction of entry retaining wall along a gob side under hard roof stratum [J]. International Journal of Rock Mechanics and Mining Sciences, 2015, 77: 115–121. DOI: https://doi.org/10.1016/j.ijrmms.2015.03.025.

[12] KAISER P K, CAI M. Design of rock support system under rockburst condition [J]. Journal of Rock Mechanics and Geotechnical Engineering, 2012, 4(3): 215–227. DOI: https://doi.org/10.3724/SP.J.1235.2012.00215.

[13] GUO W Y, TAN Y L, YU F H, ZHAO T B, HU S C, HUANG D M, QIN Z W. Mechanical behavior of rock-coal-rock specimens with different coal thicknesses [J]. Geomechanics and Engineering, 2018, 15(4): 1017–1027. DOI: https://doi.org/10.12989/gae.2018.15.4.1017.

[14] JIANG Li-shuai, KONG Peng, SHU Jia-ming, FAN Ke-gong. Numerical analysis of support designs based on a case study of a longwall entry [J]. Rock Mechanics and Rock Engineering, 2019. DOI: https://doi.org/10.1007/s00603-018-1728-2.

[15] CHEN Bing-rui, FENG Xia-ting, LI Qing-peng, LUO Ru-zhou, LI Shao-jun. Rock burst intensity classification based on the radiated energy with damage intensity at Jinping II Hydropower Station, China [J]. Rock Mechanics and Rock Engineering, 2015, 48(1): 289–303. DOI: https://doi.org/10.1007/ s00603-013-0524-2.

[16] LIU X S, TAN Y L, NING J G, LU Y W, GU Q H. Mechanical properties and damage constitutive model of coal in coal-rock combined body [J]. International Journal of Rock Mechanics and Mining Sciences, 2018, 110: 140–150. DOI: https://doi.org/10.1016/j.ijrmms.2018.07.020.

[17] CHEN L, LI P, LIU G, CHENG W, LIU Z. Development of cement dust suppression technology during shotcrete in mine

of China-A review [J]. Journal of Loss Prevention in the Process Industries, 2018, 55: 232–242. DOI: https://doi.org/10.1016/j.jlp. 2018.07.001.

[18] ZHU Guang-an, DOU Lin-ming, CAO An-ye, CAI Wu, WANG Chang-bin, LIU Zhi-gang, LI Jing. Assessment and analysis of strata movement with special reference to rock burst mechanism in island longwall panel [J]. Journal of Central South University, 2017, 24(12): 2951−2960. DOI: https://doi.org/10.1007/s11771-017-3709-0.

[19] MANOUCHEHRIAN A, CAI M. Numerical modeling of rockburst near fault zones in deep tunnels [J]. Tunnelling and Underground Space Technology, 2018, 80: 164–180. DOI: https://doi.org/10.1016/j.tust.2018.06.015

[20] HE M C, MIAO J L, LI D J, WANG C G. Experimental study on rockburst processes of granite specimen at great depth [J]. Chinese Journal of Rock Mechanics and Engineering, 2007, 26: 865–876. (in Chinese)

[21] HE M C, NIE W, ZHAO Z Y, GUO W. Experimental investigation of bedding plane orientation on the rockburst behavior of sandstone [J]. Rock Mechanics and Rock Engineering, 2012, 45(3): 311–326. DOI: https://doi.org/10.1007/s00603-011-0213-y.

[22] HE M C, JIA X N, COLI M, LIVI E, SOUSA L. Experimental study of rockbursts in underground quarrying of Carrara marble [J]. International Journal of Rock Mechanics and Mining Sciences, 2012, 52: 1–8. DOI: https://doi.org/10.1016/j.ijrmms.2012.02.006.

[23] ZHAO F, HE Man-chao. Size effects on granite behavior under unloading rockburst test [J]. Bulletin of Engineering Geology and the Environment, 2016, 76(3): 1183–1197. DOI: https://doi.org/10.1007/s10064-016-0903-5.

[24] SU Guo-shao, JIANG Jian-qing, ZHAI Shao-bin, ZHANG Gang-liang. Influence of tunnel axis stress on strainburst: An experimental study [J]. Rock Mechanics and Rock Engineering, 2017, 50(6): 1551–1567. DOI: https://doi.org/10.1007/s00603-017-1181-7.

[25] DU Kun, TAO Ming, LI Xi-bing, ZHOU Jian. Experimental study of slabbing and rockburst induced by true-triaxial unloading and local dynamic disturbance [J]. Rock Mechanics and Rock Engineering, 2016, 49(9): 3437–3453. DOI: https://doi.org/10.1007/s00603-016-0990-4.

[26] HE M C, LIU D Q, GONG W L, WANG C X, KONG J, DU S, ZHANG S. Development of a testing system for impact rockbursts [J]. Chinese Journal of Rock Mechanics and Engineering, 2014, 33: 1729–1739. (in Chinese)

[27] AKDAG S, KARAKUS M, TAHERI A, GIANG N, HE M C. Effects of thermal damage on strain burst mechanism for brittle rocks under true-triaxial loading conditions [J]. Rock Mechanics and Rock Engineering, 2018, 51(6): 1657–1682. DOI: https://doi.org/10.1007/s00603-018-1415-3.

[28] EBERHARDT E. Numerical modelling of three-dimension stress rotation ahead of an advancing tunnel face [J]. International Journal of Rock Mechanics and Mining Sciences, 2001, 38(4): 499–518. DOI: https://doi.org/10.1016/S1365-1609(01)00017-X.

[29] KAISER P K, YAZICI S, MALONEY S. Mining-induced stress change and consequences of stress path on excavation stability—A case study [J]. International Journal of Rock Mechanics and Mining Sciences, 2001, 38(2): 167–180. DOI: https://doi.org/https://doi.org/10.1016/S1365-1609(00)00038-1.

[30] MOGI K. Effect of the intermediate principal stress on rock failure [J]. Journal of Geophysical Research Atmospheres, 1967, 72(20): 5117–5131. DOI: https://doi.org/10.1029/JZ072i020p05117.

[31] CHEN Xu, TANG Chun-an, YU Jin, ZHOU Jian-feng, CAI Yan-yan. Experimental investigation on deformation characteristics and permeability evolution of rock under confining pressure unloading conditions [J]. Journal of Central South University, 2018, 25(8): 1987–2001. DOI: https://doi.org/10.1007/s11771-018-3889-2.

[32] LABUZ J F, BRIDELL J M. Reducing frictional constraint in compression testing through lubrication [J]. International Journal of Rock Mechanics and Mining Sciences and Geomechanics Abstracts, 1993, 30(4): 451–455. DOI: https://doi.org/10.1016/0148-9062(93)91726-Y.

[33] FENG X T, ZHANG X W, KONG R, WANG G. A novel Mogi type true triaxial testing apparatus and its use to obtain complete stress–strain curves of hard rocks [J]. Rock Mechanics and Rock Engineering, 2016, 49(5): 1649–1662. DOI: https://doi.org/10.1007/s00603-015-0875-y.

[34] LIU L P. Study of rockburst of drainage tunnels in JinPing II Hydropower Station [D]. Beijing: China University of Geosciences (Beijing), 2011. (in Chinese)

[35] XIE H P, JU Y, LI L Y. Criteria for strength and structural failure of rocks based on energy dissipation and energy release principles [J]. Chinese Journal of Rock Mechanics and Engineering, 2005, 24: 3003–3010. (in Chinese)

[36] TAN Yun-liang, GUO Wei-yao, GU Qing-heng, ZHAO Tong-bin, YU Feng-hai, HU Shan-chao, YIN Yan-chun. Research on the rockburst tendency and AE characteristics of inhomogeneous coal-rock combination bodies [J]. Shock and Vibration, 2016: Article ID 9271434. DOI: https://doi.org/10.1155/2016/ 9271434.

[37] ZHAO Tong-bin, GUO Wei-yao, TAN Yun-liang, YIN Yan-chun, CAI Lai-sheng, PAN Jun-feng. Case studies of rock bursts under complicated geological conditions during multi-seam mining at a depth of 800 m [J]. Rock Mechanics and Rock Engineering, 2018, 51(5) 1539–1564. DOI: https://doi.org/10.1007/s00603-018-1411-7.

[38] ZHAO Jin-hai, JIANG Ning, YIN Li-ming, BAI Li-yang. The effects of mining subsidence and drainage improvements on a waterlogged area [J]. Bulletin of Engineering Geology and the Environment, 2018. DOI: https://doi.org/10.1007/ s10064-018-1356-9.

[39] CAI M, MORIOKAB H, KAISERA P K, TASAKAC Y, KUROSEC H, MINAMIB M, MAEJIMA T. Back-analysis of rock mass strength parameters using AE monitoring data [J]. International Journal of Rock Mechanics and Mining Sciences, 2007, 44(4): 538–549. DOI: https://doi.org/10.1016/j.ijrmms. 2006.09.012.

[40] NASSERI M H B, GOODFELLOW S D, LOMBOS L, YOUNG R P. 3-D transport and acoustic properties of Fontainebleau sandstone during true-triaxial deformation experiments [J]. International Journal of Rock Mechanics and Mining Sciences, 2014, 69: 1–18. DOI: https://doi.org/10.1016/j.ijrmms. 2014.02.014.

(Edited by HE Yun-bin)

中文导读

考虑中间主应力影响的隧道开挖应力路径下大理岩应变型岩爆过程试验研究

摘要：应变型岩爆常发生于深埋隧道中，是岩爆的基本类型之一。本文利用自主研制的真三轴试验系统对大理岩试样开展隧道开挖应力路径下应变型岩爆过程试验研究。设计了两种试验路径，一种是常用的真三轴卸载岩爆试验路径，另一种是考虑隧道开挖过程中围岩中间主应力变化的新试验路径。试验过程中，应用高速摄像机记录岩样卸载临空面应变型岩爆破坏过程，并应用声发射监测系统监测岩样破坏过程中的声发射特征。试验结果表明：两种试验路径下岩样均发生了应变型岩爆破坏现象，但新试验路径下岩样应变型岩爆过程更剧烈，表明中间主应力对大理岩的岩爆行为具有显著的影响；卸载前中间主应力越大，岩样内积聚的弹性应变能越多，破坏过程中累计声发射能量越大，即岩样破坏时释放的弹性应变能越多，岩样发生岩爆破坏时弹射碎屑的总质量越大、粒度越大，破坏过程越剧烈。

关键词：应变型岩爆；真三轴试验；中间主应力；声发射；大理岩